Journal of Power Sources 266 (2014) 275–281

Contents lists available at ScienceDirect

Journal of Power Sources

journal homepage: www.elsevier.com/locate/jpowsour

Synthesis and characterization of a new layered cathode material for sodium ion batteries

Siham Doubaji [a], Mario Valvo [b], Ismael Saadoune [a, *], Mohammed Dahbi [b], Kristina Edström [b]

[a] LCME, FST Marrakech, University Cadi Ayyad, Av. A. Khattabi, BP 549, 40000 Marrakech, Morocco
[b] Depatment of Chemistry – Ångström Laboratory, Box 538, Uppsala University, SE-75121 Uppsala, Sweden

HIGHLIGHTS

- $Na_{2/3}Co_{2/3}Mn_{2/9}Ni_{1/9}O_2$ by a sol gel method.
- This layered material adopts the P2-type structure as revealed by the Rietveld analysis.
- This cathode delivers a reversible discharge capacity of 110 mAh g^{-1} with an excellent capacity retention.
- Up to 140 mAh g^{-1} could be reached if cycled between 2.0 and 4.5 V.

ARTICLE INFO

Article history:
Received 20 March 2014
Received in revised form
24 April 2014
Accepted 8 May 2014
Available online 21 May 2014

Keywords:
Energy storage
Sodium-ion batteries
Layered oxide
$Na_{2/3}Co_{2/3}Mn_{2/9}Ni_{1/9}O_2$

ABSTRACT

Owing to the high abundance of sodium and its low cost compared to lithium, sodium ion batteries have recently attracted a renewed interest as possible candidates for stationary and mobile energy storage devices. Herein, we present a new sodium ion intercalation material, $Na_xCo_{2/3}Mn_{2/9}Ni_{1/9}O_2$, which has been synthesized by a sol–gel route in air followed by a heat treatment at 800 °C for 12 h. Its structure has been studied by X-ray diffraction showing that the material crystallized in a P2-type structure (space group $P6_3/mmc$). As far as the electrochemical properties of $Na_xCo_{2/3}Mn_{2/9}Ni_{1/9}O_2$ as positive electrode are concerned, this compound offers a specific capacity of 110 mAh g^{-1} when cycled between 2.0 and 4.2 V *vs.* Na^+/Na. The electrodes exhibited a good capacity retention and a coulombic efficiency exceeding 99.4%, as well as a reversible discharge capacity of 140 mAh g^{-1} when cycled between 2.0 and 4.5 V. These results represent a further step towards the realization of efficient sodium ion batteries, especially considering that the synthesis method proposed here is simple and cost effective and that all the electrochemical measurements were carried out without any use of additives or any optimization for both the materials and the cell components.

1. Introduction

Sodium ion batteries were initially studied alongside with lithium ion (Li-ion) cells in the 80's [1–5]. However, the latter technology has been more investigated, due to the fact that lithium is the lightest metallic element and possesses the lowest redox potential ($E_{(Li+/Li)} = -3.04$ V *vs.* SHE) among solids, which confers to Li-ion batteries a high voltage and an intrinsic high energy density. Besides, the small ionic radius of Li^+ typically enables a smooth diffusion through most of the solids. Therefore, these favourable properties, coupled to the electrolyte–electrode interface problems in the case of sodium ion batteries, made the researchers focus exclusively on Li-ion cells.

Li-ion batteries are now the most common rechargeable technology in portable electronic devices and they are also regarded as possible candidates for powering future generations of hybrid and plug-in hybrid electric vehicles. In addition to the use of lithium in batteries, which represents 25–30% of its global consumption [6], this alkaline metal is also used in many other fields, thus increasing its demand each year. Therefore, the availability of lithium has attracted significant concerns lately, since it could become progressively more expensive and also because most of its natural sources are located in politically sensitive areas.

* Corresponding author. Tel.: +212 6 61 48 64 64; fax: +212 5 24 43 31 70.
E-mail addresses: i.saadoune@uca.ma, saadoune1@yahoo.fr (I. Saadoune).

http://dx.doi.org/10.1016/j.jpowsour.2014.05.042
0378-7753/

The abundance and the low cost of sodium, as well as its suitable redox potential ($E_{(Na+/Na)} = -2.71$ V *vs.* SHE) have then made the electrochemical energy storage community to investigate once again Na-ion batteries as possible replacements for lithium ones. So far, a great number of compounds have been studied as positive electrode materials for sodium ion batteries, e.g. olivines, nasicon structures and also layered oxides, since their lithium counterparts are known for their commercial application as cathodes for Li-ion cells.

2D layered transition metal oxides $NaMO_2$ (with M = Co, Mn, Ni, Cr, Fe) have been studied as cathode materials for sodium ion batteries, even if their performance is not comparable to that of their lithium analogues. Nevertheless, they could still represent a further step towards the realization of sustainable sodium ion batteries, especially if combined in more cost-effective and simpler fabrications together with non-toxic and abundant materials for the remaining cell components [7]. Unlike $LiMO_2$, $NaMO_2$ possess different crystal structures where Na is located either in octahedral or in prismatic sites between the layers of the transition metal octahedra MO_6. These structures differ in the stacking of oxygen layers with ABCABC for O3, ABBA for P2 and ABBCCA for P3 (O and P refer to the octahedral and prismatic sites of sodium, respectively) [3,8–15].

In particular, Na_xCoO_2 was investigated among these sodium oxides in 1980's demonstrating its feasibility as a cathode material for sodium ion batteries. Na_xCoO_2 crystallizes in different structures depending on the oxygen stoichiometry that depends on the oxygen pressure used during the synthesis and also on the Na amount which can vary depending on the synthesis conditions and the heat treatment temperature ($0.55 < x_{Na} < 0.60$ (P'3); $0.64 < x_{Na} < 0.74$ (P2); $x_{Na} = 0.77$ (O'3) and $x_{Na} = 1$ (O3)), where the P2-phase offers better cycle life and improved energy efficiency [2,5]. P2-Na_xCoO_2 has been reinvestigated [7,8] showing promising results with decent reversible capacity and cycleability. However, the intercalation/deintercalation of sodium ions in this material occurs by the existence of well defined steps in the voltage profile in the potential window 2.0–3.8 V *vs.* Na^+/Na. It has been reported in another work that the substitution of Co with Mn P2-$NaCo_{2/3}Mn_{1/3}O_2$ [13] stabilizes the structure, which exhibits only one voltage step at $x_{Na} = 0.5$ between 1.25 and 4.0 V, this being due to the coexistence of Co^{3+} and Mn^{4+}. However, neither the values of the capacity delivered by the material nor the coulombic efficiency were reported. The study of the structural and electrochemical properties of $NaNi_{1/3}Mn_{1/3}Co_{1/3}O_2$ was reported by Sathiya et al. [12]. This compound delivered 120 mAh g^{-1} at a current density of 12 mA g^{-1} between 2 and 3.75 V $Na_{0.63}Ni_{0.22}Co_{0.11}Mn_{0.66}O_2$, reported by Buchholz and al. [14] delivers a specific discharge capacity of 134 mAh g^{-1} at a current rate of 12 mA g^{-1} in the voltage range of 2–4.3 V. Similar compound with a slight difference in stoichiometry $Na_{0.67}Mn_{0.65}Co_{0.2}Ni_{0.15}O_2$ was reported by Yuan et al. [15]. A specific discharge capacity of 141 mAh g^{-1} was delivered by this electrode material when cycled between 2 and 4.4 V. These three compounds display high discharge capacities with good capacity retention and good rate capability. Thus, the coexistence of cobalt, manganese and nickel in the transition metal layers gives these materials their good electrochemical performances.

In this work, we have synthesized a new material, P2-$Na_xCo_{2/3}Mn_{2/9}Ni_{1/9}O_2$, by a sol gel route, in order to improve the structural and electrochemical behaviour of $NaCoO_2$ where we assume the coexistence of Co^{3+}, Mn^{4+} and Ni^{2+} [16]. The choice of substituting Co with Mn and Ni actually comes from previous works done in our group on lithium analogues [16–19] which gave excellent specific discharge capacities, low polarization and extensive cycle life. Indeed, the electrochemical study of this material proves that the Na^+ intercalation/deintercalation process is reversible and proceeds smoothly, thus demonstrating that the addition of both manganese and nickel with this stoichiometry stabilizes the structure. At the same time, this approach successfully improved the properties of the material leading to a good capacity retention during cycling and providing a high coulombic efficiency. Therefore, P2-$Na_xCo_{2/3}Mn_{2/9}Ni_{1/9}O_2$ represents a new candidate for sodium ion batteries as a positive electrode material.

2. Experimental

$Na_xCo_{2/3}Mn_{2/9}Ni_{1/9}O_2$ was synthesized by a sol gel route using sodium, cobalt, manganese, and nickel acetates in the molar ratio of 0.7:0.66:0.22:0.11 with 5% excess of sodium. The stoichiometric amounts of the precursors were mixed in distilled water and then stirred for 2 h before adding the chelating agent, which here was citric acid. The mixture was kept at 80 °C under constant stirring until a homogeneous gel was obtained. The latter was dried over night at 110 °C in order to obtain a powder. The resulting powder was ball milled and further heat-treated in a furnace at 800 °C for 12 h under air. After this, the material was stored in an Ar-filled glove box (H_2O, $O_2 < 1$ ppm).

The composition of the material $Na_xCo_{2/3}Mn_{2/9}Ni_{1/9}O_2$ was measured using Inductively Coupled Plasma (ICP) emission spectroscopy (Spectro Ciros ccd) in terms of sodium and transition metal contents. The crystalline structure of the synthesized material was characterized by X-ray diffraction (XRD) using a Bruker D8 Advance diffractometer equipped with Cu Kα radiation. The XRD pattern was collected in the 2θ range of 10–90° in a continuous scan mode with a step size of 0.01° and a constant counting time of 10 s. Lattice parameters were refined using a typical Rietveld method implemented in the FullProf program [20]. The powder morphology and the size distribution of the particles were observed by high resolution scanning electron microscopy (HR-SEM) using a Zeiss Leo 1550 scanning electron microscope equipped with a X-MAX EDX probe (Oxford Instruments) for elemental analysis. Infrared (IR) measurements were carried out via a Perkin–Elmer Spectrum One FT-IR spectrometer equipped with an attenuated total reflectance (ATR) probe. The resulting spectra were collected in the wavenumber range spanning from 650 to 3000 cm^{-1}.

For the electrochemical measurements, the positive composite electrodes were prepared by mixing 75 wt% of the active material with 15 wt% of carbon black (Super P) conductive additive and 10 wt% of polyvinylidene fluoride (PVDF) binder using *N*-methyl-2-pyrrolidone (NMP) as solvent. The slurry was then casted on an Al foil and dried at 60 °C for 3 h in a convection oven. The electrodes were cut into 20 mm disks by a precision perforator (Hohsen) and dried over night at 120 °C in a vacuum oven within the Ar-filled glove box (M-Braun). The active electrode materials have an average weight of 5 mg. Sodium metal was used as both reference and counter electrode by cutting, rolling and pressing sodium lumps into thin plates. A thin membrane (Solupore) was used as separator between the sodium plate and the working electrode. The electrodes were assembled and vacuum-sealed in the Ar-filled glove box into "coffee-bag" (polymer laminated aluminium pouch) cells [21] with 0.5 M $NaPF_6$ electrolyte dissolved in PC (polycarbonate). All the electrochemical measurements were carried out at room temperature (25 °C) via a VMP2 (Bio-Logic) equipment. The charge/discharge studies were performed galvanostatically at a current rate of C/20 (i.e. 12.6 mA g^{-1}), where a period of 20 h is required to remove one sodium ion. In particular, two different cut-off voltages were used: the first one between 2.0 and 4.2 V and the second one between 2.0 and 4.5 V. The rate capability test with different constant current rates, C/*n* (with $n = 20, 10, 5, 2, 1, 0.5$), was performed as well. Cyclic voltammetry (CV) measurements were carried out at a typical scan rate of

0.1 mV s^{-1} between 2.0 and 4.2 V *vs.* Na^+/Na. A reproducibility was checked for all the experiments, including the synthesis, by repeating all the steps at least twice.

3. Results and discussion

3.1. Structural, compositional and morphological study

The elemental composition of $Na_xCo_{2/3}Mn_{2/9}Ni_{1/9}O_2$ was investigated using the ICP method and the results were 0.69:0.66:0.22:0.11 M composition, respectively, for Na:Co:Mn:Ni, which is consistent with the expected stoichiometry. The sodium amount was further confirmed by the Rietveld refinement, and it will be assumed to be 2/3 in the following sections.

The XRD pattern and the Rietveld-refined results of the as-prepared material are depicted in Fig. 1. The diffractogram clearly shows a single phase where no crystalline impurities were observed. All Bragg diffraction lines indicate that $Na_{2/3}Co_{2/3}Mn_{2/9}Ni_{1/9}O_2$ crystallizes in the hexagonal layered structure (P2-type structure) with the space group $P6_3/mmc$. The unit cell parameters obtained from the structural refinement are $a = 2.8274(7)$ Å and $c = 11.0553(6)$ Å.

The P2-type structure has ABBA oxygen packing where the transition metal ions (i.e. cobalt, manganese and nickel) occupy randomly the octahedral sites, while the sodium ions reside in two different trigonal prismatic sites, thus forming a layered structure where Na^+ is sandwiched between (MO_2) slabs (M = Co, Mn, Ni). The transition metals are located in 2a site (0,0,0), the oxygen in the site 4f (2/3,2/3,*z*) where *z* was found to be 0.089 using the Rietveld refinement. On the other hand, the sodium is located both in the site 2b (0,0,1/4), where the prismatic NaO_6 share faces with the MO_6 octahedra (Na_1), and in the site 2d (2/3,1/3,1/4) where it only shares edges (Na_2). Due to the electrostatic repulsion between the transition metal ions and sodium ions in the 2b site, this site is expected to be less stable compared to the 2d site for sodium. Fig. 2 represents the P2-type structure of $Na_{2/3}Co_{2/3}Mn_{2/9}Ni_{1/9}O_2$. It should be noticed that in the case of the Li_xMO_2 phases (M:Co, Ni, Mn), all the synthesis procedures performed at high temperatures, lead to stoichiometric materials ($x \approx 1$) [16–19]. Upon lithium extraction at room temperature, these phases undergo some structural transitions without changing the octahedral

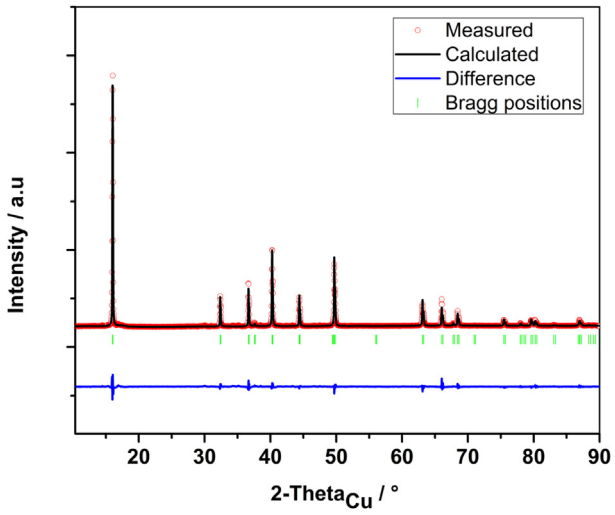

Fig. 1. Observed and calculated XRD profiles for the $Na_{2/3}Co_{2/3}Mn_{2/9}Ni_{1/9}O_2$ phase: (red) observed; (black) calculated; (blue) difference plot; (green bars) Bragg reflections. (For interpretation of the references to colour in this figure legend, the reader is referred to the web version of this article.)

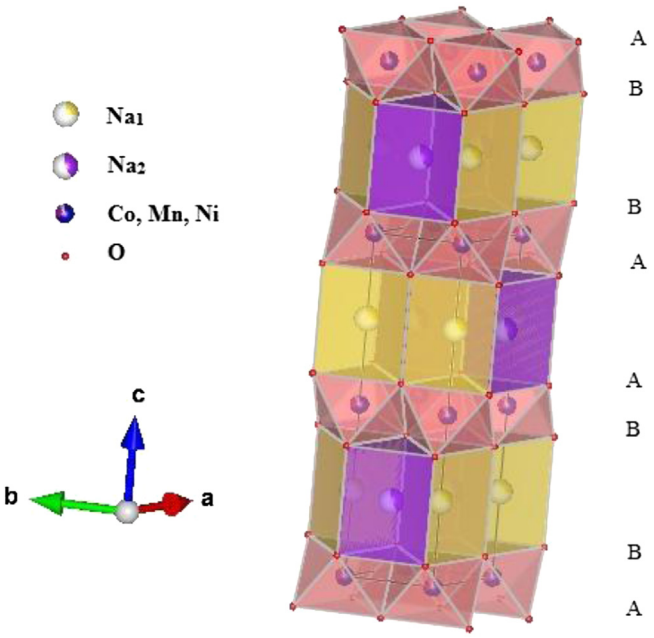

Fig. 2. Illustration of the P2-structure, presenting the two different NaO_6 prisms.

environment of the lithium. This could be related to the high stabilization of lithium in an octahedral site as a result of its smaller size compared to sodium. Nevertheless, in the case of sodium phases, the high iconicity of the Na–O bonding comparing to Li–O, permits many possible gliding motion of the $(MO_2)_n$ slabs during the thermal treatment or upon sodium removal. So, the structure of Na_xMO_2 depends on the annealing temperature, the oxygen pressure and the amount of sodium ions.

The distribution of the sodium ions in the two sites was identified by the Rietveld method. The refined parameters are summarized in Table 1. Note that B_{iso} factors for sodium ions are relatively high indicating a high mobility of this ion within the structure. This point could be considered as an advantage, as the sodium extraction/insertion reaction requires a good ionic conduction of the host material.

The SEM images at different magnification, presented in Fig. 3, confirm the hexagonal layered structure of the compound, as it is easily noticed from the characteristic morphology of the powders.

Table 1
Crystallographic parameters of the $Na_{2/3}Co_{2/3}Mn_{2/9}Ni_{1/9}O_2$ refined by Rietveld analysis. Conventional reliability factors of the refinements are given as well.

Space group						
$P6_3/mmc$						
$a_{hex.} = 2.8274(7)$ Å						
$c_{hex.} = 11.0553(6)$ Å						
Atom	Wyckoff positions				Occupancy	B Å^{-2}
Na_1	2b	0	0	1/4	0.279(7)	3.4(7)
Na_2	2d	2/3	1/3	1/4	0.410(4)	2.2(6)
Co	2a	0	0	0	2/3	0.25
Mn	2a	0	0	0	2/9	0.25
Ni	2a	0	0	0	1/9	0.25
O	4f	1/3	2/3	0.089(6)	1.000	1.6(3)
Profile parameters						
$\eta_0 = 0.40(5)$						
$X = 0.0075(1)$						
$U = 0.061(9)$						
$V = -0.038(5)$						
$W = 0.013(8)$						
Conventional Rietveld R-factors for points with Bragg contribution						
$R_{wp} = 10.4\%$; $R_B = 2.87\%$						

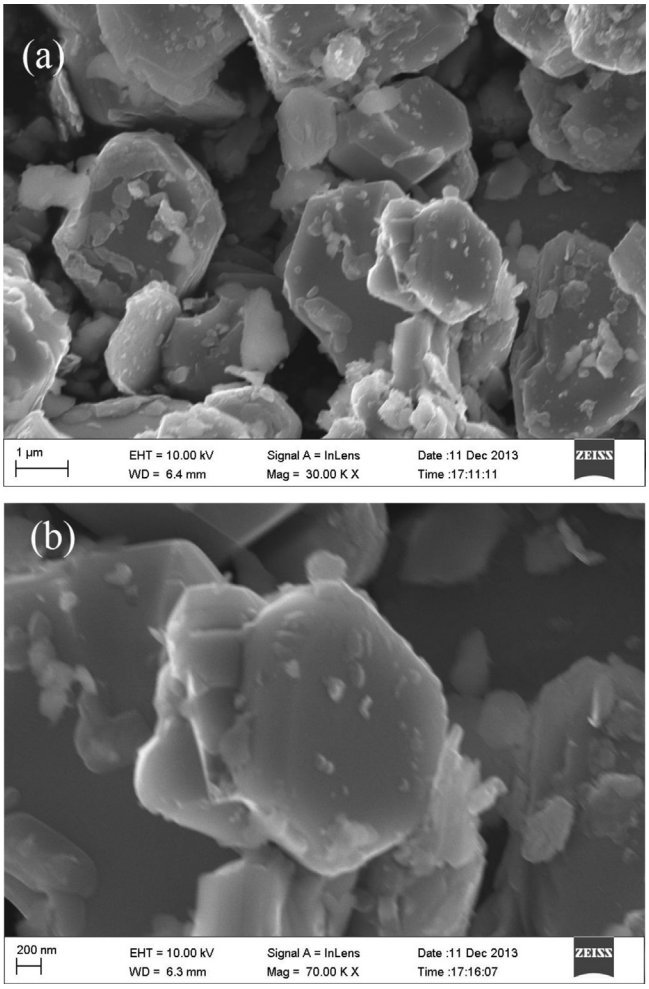

Fig. 3. SEM images taken at different magnifications for $Na_{2/3}Co_{2/3}Mn_{2/9}Ni_{1/9}O_2$ powders. Note the typical hexagonal-like shape of some large particles in both micrographs.

The typical size of the particles is found to be between 1 and 3 µm. Some rough features are noticed on the surface of the particles, which here are believed to be due to the presence of sodium carbonate. Indeed, they can originate from the sodium being extracted from the structure by exposure to air [12,14,22]. In order to confirm this hypothesis, IR measurements were performed on the pristine material (See the Supporting Information). The presence of two bonds at 863 cm^{-1} (corresponding to δ(O–C–O)) and at 1450 cm^{-1} (corresponding to υ(C–O)), confirms the existence of sodium carbonate on the surface of the compound [12].

Moreover, the chemical maps obtained during the elemental analysis via SEM/EDX show an even distribution for sodium on the surface of the synthesized powders. Also the distribution of the other elements present in the compound (i.e. Co, Mn, Ni, O and C) appeared homogeneous. Therefore, Na was distributed quite homogeneously in the compound, irrespectively of the slight surface contamination with Na_2CO_3 due to air exposure. Thus, in order to prevent such a contamination, the studied samples were kept inside the inert atmosphere of the glove box.

3.2. Electrochemical tests

The open circuit voltage (OCV) of all the cells with $Na_{2/3}Co_{2/3}Mn_{2/9}Ni_{1/9}O_2$ as the cathode material was 2.84 V (*vs.* Na^+/Na). Fig. 4 shows the potential versus the amount of deintercalated sodium (i.e. V *vs.* Na^+/Na and *x* in $Na_xCo_{2/3}Mn_{2/9}Ni_{1/9}O_2$) for the first

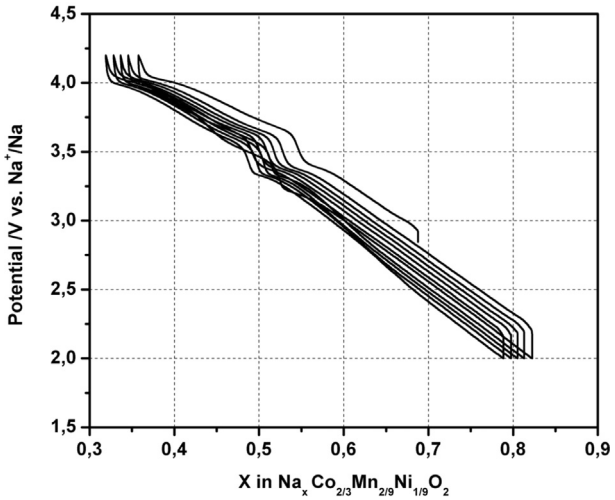

Fig. 4. Galvanostatic charge/discharge profiles for the first five cycles undergone by the $Na_{2/3}Co_{2/3}Mn_{2/9}Ni_{1/9}O_2$ electrode in the potential window 2–4.2 V *vs.* Na^+/Na at a rate of C/20 (i.e. 12.6 mA g^{-1}). Note that the horizontal axis represents the storage capacity of the compound, i.e. *x* moles of deintercalated/intercalated Na^+ in $Na_xCo_{2/3}Mn_{2/9}Ni_{1/9}O_2$.

five cycles between 2.0 and 4.2 V using a rate of C/20 (i.e. a current of 12.6 mA g^{-1}). The shape of the curves clearly shows that the sodium extraction/insertion in the studied material is reversible with three distinct plateaus at about 3.4, 3.6 and 4.0 V. The amount of sodium removed after the first charge is 0.32 (i.e. $Na_{0.35}Co_{2/3}Mn_{2/9}Ni_{1/9}O_2$), which corresponds to delivering a specific capacity of 80 mAh g^{-1}. At the end of the subsequent discharge, the intercalated Na^+ amount is 0.42 (i.e. $Na_{0.77}Co_{2/3}Mn_{2/9}Ni_{1/9}O_2$), thus increasing the initial content of sodium present in the compound and consequently providing a higher discharge capacity of about 107 mAh g^{-1}. The shape of the curve from 2.0 V to 3.4 V demonstrates a solid solution, however, at 3.4 V a jump of the voltage is noticed, which could be explained by the existence of a structural or/and electronic transition at these potentials [13]. Note that the behaviour of the lithium-based electrode materials $LiMO_2$, such structural or/and electronic transitions accompanied by potential plateau are not habitually observed as a result of the high covalency of the Li–O bonding. In general, a continuous evolution of the potential with composition is obtained [17].

A galvanostatic test was performed with a rate of C/20 (i.e. 12.6 mA g^{-1}) between 2.0 and 4.2 V for 90 cycles in order to study the evolution of the capacity of the material during cycling, which is represented in Fig. 5. The material offers a reversible capacity of 110 mAh g^{-1} showing a good capacity retention, a loss of only 11% of the initial capacity after 90 cycles and a very good coulombic efficiency exceeding 99.4%. It was also noticed that the capacity started to increase from 107 to 110 mAh g^{-1} during the first 10 cycles. After that, the specific capacity gradually stabilized and also the coulombic efficiency after the first cycle increased from about 98.0% to 99.4% remaining stable upon subsequent cycling. This can be explained by the fact that the battery cycling progressively stabilizes as the sodium begins to intercalate smoothly into the compound after the first few cycles.

The rate capability test started with the first nine cycles at a rate of C/20 (12.6 mA g^{-1}) followed by six cycles at the increasing rates: C/10 (25.2 mA g^{-1}), C/5 (50.4 mA g^{-1}), C/2 (126.3 mA g^{-1}), 1C (252.6 mA g^{-1}), and 2C (505.2 mA g^{-1}), respectively, to lastly return to C/20 with six cycles. The evolution of the capacity upon progressive cycles and the associated coulombic efficiency are presented in Fig. 6. $Na_{2/3}Co_{2/3}Mn_{2/9}Ni_{1/9}O_2$ clearly showed promising

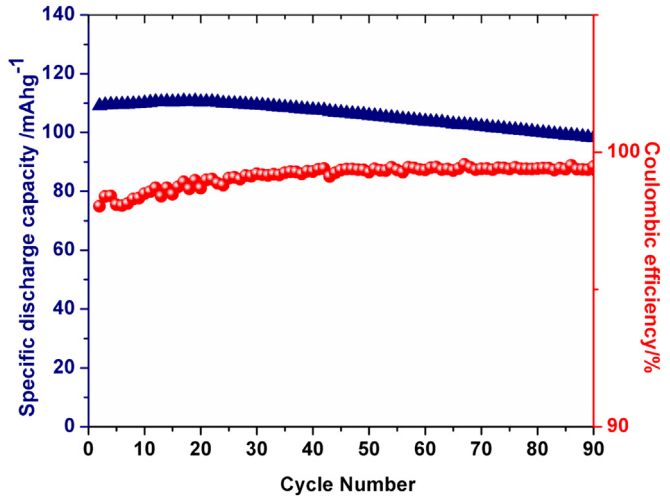

Fig. 5. Evolution of the discharge capacity and the coulombic efficiency of the $Na_{2/3}Co_{2/3}Mn_{2/9}Ni_{1/9}O_2$ electrode with the cycle number upon galvanostatic cycling at a rate of C/20 (i.e. 12.6 mA g^{-1}).

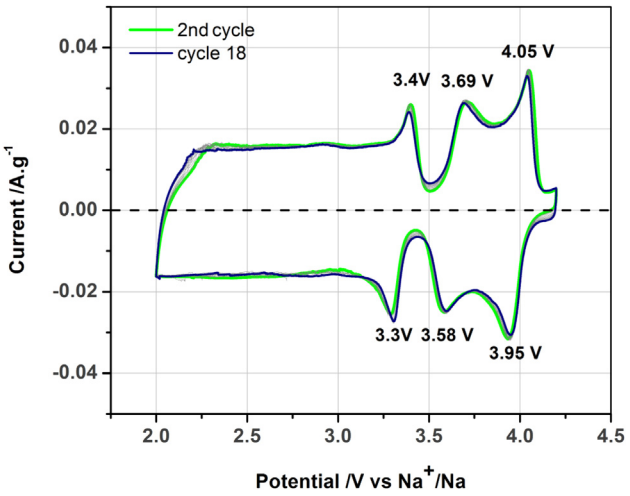

Fig. 7. Cyclic voltammogram for the $Na_{2/3}Co_{2/3}Mn_{2/9}Ni_{1/9}O_2$ electrode cycled at a scan rate of 0.1 mV s^{-1} between 2 and 4.2 V. Note that seventeen consecutive cycles are reported in the same plot.

results also in this preliminary test. This compound indeed offered a series of specific capacities of: 105 mA g^{-1} at C/10, 104 mA g^{-1} at C/5, 96 mA g^{-1} at C/2, 77 mA g^{-1} at 1C, and 67 mA g^{-1} at 2C, respectively. Finally, it fully recovered the initial capacity of 110 mA g^{-1} in the last cycles performed at C/20 displaying an excellent coulombic efficiency, which overall varied between 99 and 95% during the entire rate capability test.

The cyclic voltammogram yielded by the $Na//Na_xCo_{2/3}Mn_{2/9}Ni_{1/9}O_2$ electrochemical cell scanned between 2.0 and 4.2 V *vs.* Na^+/Na at a rate of 0.1 mV s^{-1} is presented in Fig. 7. Three anodic peaks (i.e. Na^+ deintercalation) are observed with central positions respectively at 3.4, 3.69 and 4.05 V corresponding, on their turn, to the three cathodic peaks seen at 3.3, 3.58 and 3.95 V during the reductive part of the cycle (i.e. Na^+ intercalation). It is clearly noticed that these couples of redox peaks are rather symmetric in shape and extension. Only a small separation in voltage exists between each of them, thus indicating that the various intercalation/deintercalation processes are reversible and do not suffer from any significant energy loss in each cycle at such scan rate. Indeed, only a slight shift of the anodic peaks towards higher potentials and a similar one for the cathodic features towards lower voltages is observed. This confirms the high stability and reversibility of the compound and also helps in decreasing the polarization with cycling. The benefits related to these features can be clearly seen also in the evolution of the coulombic efficiency presented in Fig. 5.

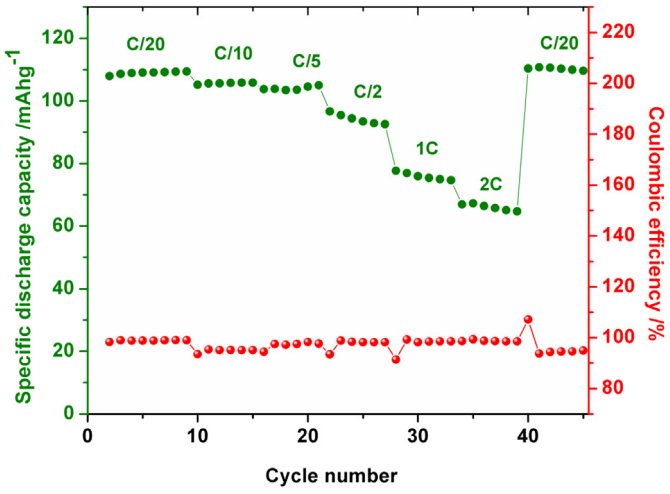

Fig. 6. Evolution of the specific discharge capacity and the coulombic efficiency during galvanostatic cycling of the $Na_{2/3}Co_{2/3}Mn_{2/9}Ni_{1/9}O_2$ electrode between 2.0 and 4.2 V *vs.* Na^+/Na at different C-rates. The first nine cycles were performed at C/20 (i.e. 12.6 mA g^{-1}). The cycles comprised between 10 and 39 illustrate the behaviour of the electrode at increasing C-rates, namely C/10 (25.2 mA g^{-1}), C/5 (50.4 mA g^{-1}), C/2 (126.3 mA g^{-1}), 1C (252.6 mA g^{-1}), and 2C (505.2 mA g^{-1}). From cycle no. 40, the electrode was once again subjected to a C/20 rate.

The shape of the peaks in the cyclic voltammogram confirms also the origin of the capacity retention observed upon galvanostatic cycling. In earlier studies of $NaMO_2$ (with M = Co, Mn, Ni) structures, a multitude of redox peaks were observed in their associated CV analyses, especially for the simple compounds having only one transition metal, such as Na_xCoO_2 and $NaNiO_2$ [7,8,23]. As a matter of fact here we have only three peaks, which confirms that the added transition metals stabilize the structure allowing for a smooth sodium intercalation/deintercalation process. The latter leads to the good capacity retention and the high coulombic efficiency observed in this material even in absence of any optimization for both the electrode formulation and the electrolyte.

Looking back at the redox features in the voltammogram in Fig. 7, it is worth mentioning that in the O3-type structure compounds (α-$NaFeO_2$ type structure), the CV peaks correspond to phase transitions [9,12] where the different phases differ from each other by a gliding of the oxide layers. For the P2-type structure, however, an in-situ XRD study [24] showed that the only transition that occurs is that causing the change from the P2 to the O2 phase. In fact, O2-type stacking faults started to appear in the P2-type structure in the XRD pattern when $x_{Na} \approx 1/3$. The coexistence of these two phases was identified when $x_{Na} < 1/3$. The P2–O2 phase transition is then represented by a pronounced oxidative peak at about 4.2 V in the cyclic voltammogram. However, we do not observe here this transition in such potential window, since the initial amount of sodium in the compound was $x_{Na} = 2/3$ and in the first charge only 0.32 mol of Na^+ were extracted. All the peaks present in the cyclic voltammogram are reported in the literature and they are related to the different alignments and staging of the sodium layers occurring when the sodium ions are deintercalated. The same plateau is noticed also in similar P2 compounds [14,15]. It should be noticed that an in-situ XRD study of the $Na_xCo_{2/3}Mn_{2/9}Ni_{1/9}O_2$ samples is in progress in order to deeply elucidate the sodium extraction/insertion mechanism.

Note that the oxidation states of the transition metals in $Na_{2/3}Co_{2/3}Mn_{2/9}Ni_{1/9}O_2$ are expected to be respectively Co^{3+}, Co^{4+}, Mn^{4+} and Ni^{2+} [13–16]. The Mn^{3+}/Mn^{4+} redox couple was found to be active in similar compounds [14,15] and it is manifested by a CV peak between 2 and 3 V which is not the case for our compound. In particular, the capacity can be generated from the oxidation of Co^{3+} to Co^{4+} or Ni^{2+} to Ni^{4+} via Ni^{3+}, as well as from both oxidative processes at the same time.

Another galvanostatic cycling experiment was also performed between 2.0 and 4.5 V in order to observe the electrochemical behaviour of the material upon charge/discharge in such high voltage region. Fig. 8 shows the profile of the potential (i.e. V *vs.* Na^+/Na) versus the amount of sodium (i.e. *x* in $Na_xCo_{2/3}Mn_{2/9}Ni_{1/9}O_2$) for the first five cycles run between 2.0 and 4.5 V using a rate of C/20 (i.e. 12.6 mA g^{-1}). The shape of the charge/discharge curves shows that the electrochemical process is still reversible even at this high upper cut-off voltage and a new plateau is observed at 4.3 V. Deep charging of $Na_xCo_{2/3}Mn_{2/9}Ni_{1/9}O_2$ to 4.5 V gives a first specific charge capacity of 125 mAh g^{-1} corresponding to a removal of 0.5 Na^+. In the subsequent discharge, an amount of 0.55 Na^+ is inserted in the material, which corresponds to a specific discharge capacity of 140 mAh g^{-1}. The evolution of the discharge capacity and the coulombic efficiency during cycling are presented in Fig. 9. The new plateau observed at 4.3 V is expected to result from the transition of the P2 to the O2 phase, as earlier mentioned. The extent of the new plateau in the first charge accounts for about 40 mA g^{-1} and in the first discharge for approximately 28 mA g^{-1}. In the second charge and discharge it accounts for 36 mA g^{-1} and 20 mA g^{-1}, respectively. Therefore, some doubts still remain about the complete reversibility of the reactions taking place in correspondence of this high voltage plateau. Possible electrolyte degradation at such a high potential could be the origin of this phenomenon.

Fig. 10 shows a comparison of the cycleability of $Na_xCo_{2/3}Mn_{2/9}Ni_{1/9}O_2$ when subjected to the same C/20 rate using these two different cut-off voltages, i.e. 2.0–4.2 V and 2.0–4.5 V. In the first two cycles the behaviour is similar and both the discharge capacities and the coulombic efficiency start to increase in both cases. Nevertheless, after this initial stage, a capacity fading is observed for the cycling of the compound with the higher cut-off voltage of 4.5 V.

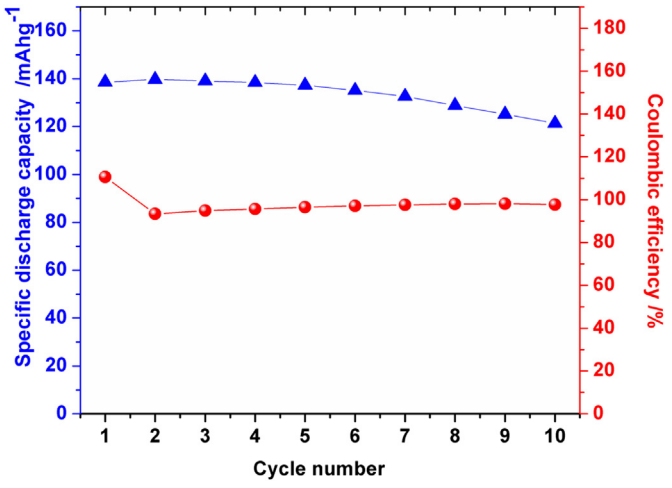

Fig. 9. Evolution of the discharge capacity and the coulombic efficiency of the $Na_{2/3}Co_{2/3}Mn_{2/9}Ni_{1/9}O_2$ electrode upon galvanostatic cycling between 2.0 and 4.5 V *vs.* Na^+/Na at C/20.

Although this irreversibility can be explained by some changes or distortions in the structure, due to the gliding of the transition metal layers caused by the high voltage, the decomposition of the electrolyte by oxidation still remains the most probable cause. In fact, the electrochemical cycling has been carried out here without using any additives in the electrolyte. In this respect, Komaba et al. [25] reported that the addition of FEC (FluoroEthylene Carbonate) in the electrolyte increases the capacity retention and the coulombic efficiency when working at high voltages.

Finally, it is possible to state that a synthesis of the same material with a lower amount of sodium might be a good way to increase the capacity at lower voltages, since the capacity gained by $Na_{2/3}Co_{2/3}Mn_{2/9}Ni_{1/9}O_2$ upon charge to 4.5 V is mostly generated from the plateau related to the P2–O2 transition.

4. Conclusions

In summary, we have synthesized a novel layered sodium ion compound with the formula $Na_{2/3}Co_{2/3}Mn_{2/9}Ni_{1/9}O_2$ by a sol gel

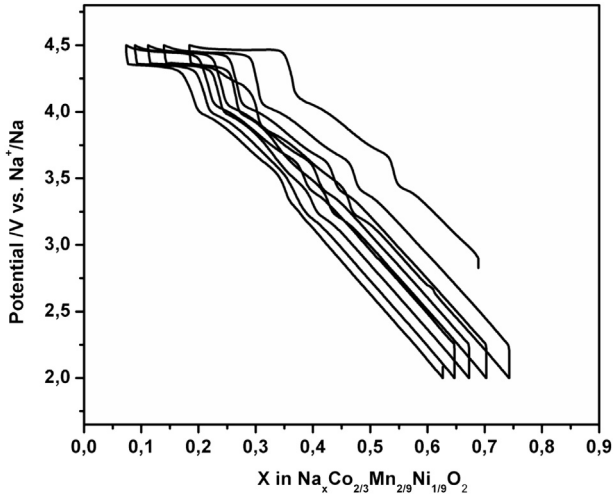

Fig. 8. Galvanostatic charge/discharge profiles for the first five cycles of the $Na_{2/3}Co_{2/3}Mn_{2/9}Ni_{1/9}O_2$ electrode cycled between 2.0 and 4.5 V *vs.* Na^+/Na at C/20 (i.e. 12.6 mA g^{-1}). The stoichiometric amount of Na^+ released and incorporated by the compound in its structure is reported on the horizontal axis of the graph and is directly related to its specific capacity.

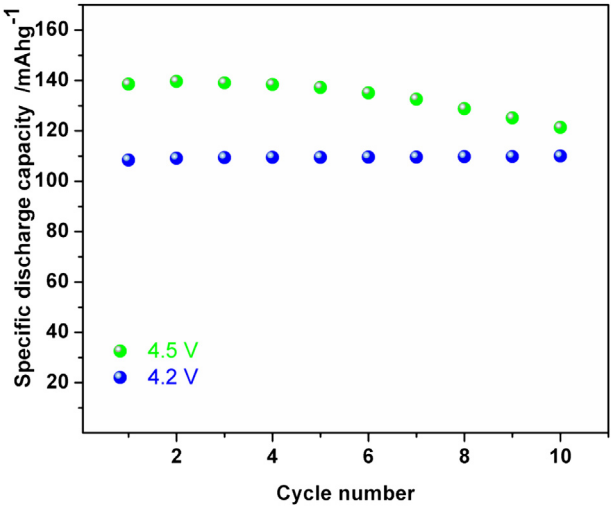

Fig. 10. Comparison of the specific discharge capacities provided by the $Na_{2/3}Co_{2/3}Mn_{2/9}Ni_{1/9}O_2$ electrodes upon galvanostatic cycling (10 cycles) at C/20 using two different upper cut-off voltages (i.e. 4.2 V and 4.5 V). Note the different trend of the data points related to these two cases.

method followed by a heat treatment under air. This new cathode material is able to deliver a specific discharge capacity of 110 mAh g^{-1} when cycled between 2.0 and 4.2 V, showing an excellent capacity retention and a high coulombic efficiency. This result is clearly promising, especially considering that the electrodes, the electrolyte and the entire cell assembly were not optimized. Some other limitations in the electrode material could be eventually minimized by further tuning its synthesis process and its coating.

The good performance of the material is due to the combination of the three transition metals: cobalt, manganese and nickel, where their coexistence is shown to significantly stabilize the structure allowing a smooth intercalation/deintercalation process for sodium.

The material delivered a high reversible capacity of 140 mAh g^{-1} when cycled between 2.0 and 4.5 V. However, at this high voltage the material suffers from a remarkable capacity fading likely caused by the decomposition of the electrolyte. Having an additive in the electrolyte could be a simple route to achieve a stabilization of the capacities upon cycling in such high voltage range. Thus, P2-$Na_{2/3}Co_{2/3}Mn_{2/9}Ni_{1/9}O_2$ can be considered a new interesting candidate as a viable positive electrode for Na-ion battery applications.

Acknowledgements

This work has been supported by the Swedish Research Council (contract 2012-4681) and the strategic research area StandUp for Energy. Mr Henrik Eriksson is gratefully acknowledged for his support during these experiments. Ms S. Doubaji is grateful to CNRST (Morocco) for the scholarship N° (H003/005).

Appendix A. Supplementary data

Supplementary data related to this article can be found at http://dx.doi.org/10.1016/j.jpowsour.2014.05.042.

References

[1] C. Delmas, J.J. Braconnier, P. Hagenmuller, Phys. B+C 99 (1980) 81.
[2] C. Delmas, J.J. Braconnier, C. Fouassier, P. Hagenmuller, Solid State Ionics 3–4 (1981) 165.
[3] A. Mendiboure, C. Delmas, P. Hagenmuller, J. Solid State Chem. 57 (1985) 323.
[4] J.M. Tarascon, G.W. Hull, Solid State Ionics 22 (1986) 85.
[5] L.W. Shacklette, T.R. Jew, L. Townsend, J. Electrochem. Soc. 135 (1988) 2669.
[6] J.M. Tarascon, Nat. Chem. 2 (2010) 510.
[7] M. Valvo, F. Lindgren, U. Lafont, F. Björefors, K. Edström, J. Power Sources 245 (2014) 967.
[8] R. Berthelot, D. Carlier, C. Delmas, Nat. Mater. 10 (2011) 74.
[9] S. Komaba, T. Nakayama, A. Ogata, T. Shimizu, C. Takei, S. Takada, A. Hokura, I. Nakai, ECS Trans. 16 (2009) 43.
[10] I. Saadoune, A. Maazaz, M. Ménétrier, C. Delmas, J. Solid State Chem. 122 (1996) 111.
[11] N. Yabuuchi, M. Kajiyama, J. Iwatate, H. Nishikawa, S. Hitomi, R. Okuyama, R. Usui, Y. Yamada, S. Komaba, Nat. Mater. 11 (2012) 512.
[12] M. Sathiya, K. Hemalatha, K. Ramesha, J.M. Tarascon, A.S. Prakash, Chem. Mater. 24 (2012) 1846.
[13] D. Carlier, J.H. Cheng, R. Berthelot, M. Guignard, M. Yoncheva, R. Stoyanova, B.J. Hwang, C. Delmas, Dalton Trans. 40 (2011) 9306.
[14] D. Buchholz, A. Moretti, R. Kloepsch, S. Nowak, V. Siozios, M. Winter, S. Passerini, Chem. Mater. 25 (2013) 142.
[15] D. Yuan, W. He, F. Pei, F. Wu, Y. Wu, J. Qian, Y. Cao, X. Aib, H. Yang, J. Mater. Chem. A 1 (2013) 3895.
[16] Y. Bentaleb, I. Saadoune, K. Maher, L. Saadi, K. Fujimoto, S. Ito, J. Power Sources 195 (2010) 1510.
[17] A. Mahmoud, I. Saadoune, J.M. Amarilla, R. Hakkou, Electrochim. Acta 56 (2011) 4081.
[18] A. Mahmoud, M. Yoshita, I. Saadoune, J. Broetz, K. Fujimoto, S. Ito, Mater. Res. Bull. 47 (2012) 1936.
[19] M. Dahbi, I. Saadoune, T. Gustafsson, K. Edström, Solid State Ionics 203 (2011) 37.
[20] J. Rodriguez-Carvajal, Fullprof, Program for Rietveld Refinement, Version 3.7, LLB JRC, 1997.
[21] T. Gustafsson, J.O. Thomas, R. Koksbang, G.C. Farrington, Electrochim. Acta 37 (1992) 1639.
[22] B. Mortemard de Boisse, D. Carlier, M. Guignard, C. Delmas, J. Electrochem. Soc. 160 (4) (2013) 569.
[23] P. Vassilaras, X. Ma, X. Li, G. Ceder, J. Electrochem. Soc. 160 (2013) 207.
[24] Z. Lu, J.R. Dahn, J. Electrochem. Soc. 148 (11) (2001) 1225.
[25] S. Komaba, N. Yabuuchi, T. Nakayama, A. Ogata, T. Ishikawa, I. Nakai, Inorg. Chem. 51 (2012) 6211.